Sinha, N. D., Biernat, J., McManus, J., & Koster, H. (1984) *Nucleic Acids Res. 12*, 4539-4557.
Sobell, H. M. (1972) *Proc. Natl. Acad. Sci. U.S.A. 69*, 2483-2487.
Soumpasis, D. M., & Jovin, T. M. (1987) in *Nucleic Acids and Molecular Biology* (Eckstein, F., & Lilley, D. M. J., Eds.) pp 85-111, Springer-Verlag, Berlin Heidelberg.
Spencer, R. D., & Weber, G. (1969) *Ann. Acad. Sci. Fenn., Ser. A2 158*, 361.
Steinberg, I. Z. (1968) *J. Chem. Phys. 48*, 2411-2413.
Stryer, L. (1978) *Annu. Rev. Biochem. 47*, 819-846.
Timsit, Y., Westhof, E., Fuchs, R. P. P., & Moras, D. (1989) *Nature 341*, 459-462.
Valeur, B. (1989) in *Fluorescent Biomolecules: Methodologies and Applications* (Reinhart, D. M. J. a. G. D., Ed.) pp 269-303, Plenum Press, New York.
von Kitzing, E., Lilley, D. M. J., & Diekmann, S. (1990) *Nucleic Acids Res. 18*, 2671-2683.

Backbone Dynamics of Calcium-Loaded Calbindin D_{9k} Studied by Two-Dimensional Proton-Detected ^{15}N NMR Spectroscopy†

Johan Kördel,‡ Nicholas J. Skelton, Mikael Akke,‡ Arthur G. Palmer, III,* and Walter J. Chazin*
Department of Molecular Biology, The Scripps Research Institute, La Jolla, California 92037
Received December 16, 1991; Revised Manuscript Received March 11, 1992

ABSTRACT: Backbone dynamics of calcium-loaded calbindin D_{9k} have been investigated by two-dimensional proton-detected heteronuclear nuclear magnetic resonance spectroscopy, using a uniformly ^{15}N enriched protein sample. Spin–lattice relaxation rate constants, spin–spin relaxation rate constants, and steady-state $\{^1H\}$–^{15}N nuclear Overhauser effects were determined for 71 of the 72 backbone amide ^{15}N nuclei. The relaxation parameters were analyzed using a model-free formalism that incorporates the overall rotational correlation time of the molecule, and a generalized order parameter (S^2) and an effective internal correlation time for each amide group. Calbindin D_{9k} contains two helix–loop–helix motifs joined by a linker loop at one end of the protein and a β-type interaction between the two calcium-binding loops at the other end. The amplitude of motions for the calcium-binding loops and the helices are similar, as judged from the average S^2 values of 0.83 ± 0.05 and 0.85 ± 0.04, respectively. The linker region joining the two calcium-binding subdomains of the molecule has a significantly higher flexibility, as indicated by a substantially lower average S^2 value of 0.59 ± 0.23. For residues in the linker loop and at the C-terminus, the order parameter is further decomposed into separate order parameters for motional processes on two distinct time scales. The effective correlation times are significantly longer for helices I and IV than for helices II and III or for the calcium-binding loops. Residue by residue comparisons reveal correlations of the order parameters with both the crystallographic *B*-factors and amide proton exchange rates, despite vast differences in the time scales to which these properties are sensitive. The order parameters are also utilized to distinguish regions of the NMR-derived three-dimensional structure of calbindin D_{9k} that are poorly defined due to inherently high flexibility, from poorly defined regions with average flexibility but a low density of structural constraints.

Calbindin D_{9k} is a small calcium-binding protein structurally homologous to the globular domains of calmodulin (CaM)[1] and troponin C (TnC). These proteins belong to the superfamily of proteins that bind Ca^{2+} ions through a common structural motif consisting of a calcium-binding loop flanked by two helices, termed the EF-hand (Kretsinger, 1987). The EF-hands generally occur in pairs, with a parallel arrangement as detailed in Figure 1. Cooperativity in the binding of calcium has been observed for some members of the CaM superfamily and has been attributed to the β-type interaction between the two calcium-binding loops (Seamon & Kretsinger, 1983; Linse et al., 1987). The binding of Ca^{2+} ions has been proposed to result in substantial structural rearrangements of the helices (Herzberg et al., 1986), which changes the nature of the interactions of these proteins with their target molecules. The proposed structural rearrangements provide a molecular mechanism for the activation of CaM [for a review, see Manalan and Klee (1984)] and TnC (Potter & Johnson, 1982). The best available model for structural rearrangements upon calcium binding is based on a comparison of the (apo) N-terminal and (Ca^{2+}-loaded) C-terminal domains in the TnC crystal structure (Herzberg et al., 1986). This model has not been directly verified or refined because none of the proteins in the calmodulin superfamily have been crystallized with *different* levels of calcium loading. Structure determination *in solution* by NMR circumvents the need for crystallization and therefore is being applied to determine the structural

† This work was supported by the National Institutes of Health (Grant GM 40120 to W.J.C.), The American Cancer Society (fellowship JFRA-294 to W.J.C.), the National Science Foundation (postdoctoral fellowship CHE-8907510 to A.G.P.), the Swedish Natural Science Research Council (graduate fellowships to J.K. and M.A.), and the Royal Swedish Academy of Sciences (travel grant to J.K.).
* To whom correspondence should be addressed.
‡ Permanent address: Department of Physical Chemistry 2, Chemical Centre, University of Lund, S-221 00 Lund, Sweden.

[1] Abbreviations: P43G, recombinant bovine calbindin D_{9k} mutant with Pro43 substituted by glycine; CaM, calmodulin; TnC, troponin C; NMR, nuclear magnetic resonance; 2D, two-dimensional; NOE, nuclear Overhauser effect; NOESY, two-dimensional NOE spectroscopy; R_1, spin–lattice or longitudinal relaxation rate constant; R_2, spin–spin or transverse relaxation rate constant; CSA, chemical shift anisotropy; INEPT, insensitive nuclei enhanced by polarization transfer; CPMG, Carr–Purcell–Meiboom–Gill; TPPI, time-proportional phase incrementation; FID, free induction decay; RMS, root mean square; ANOVA, analysis of variance.

0006-2960/92/0431-4856$03.00/0

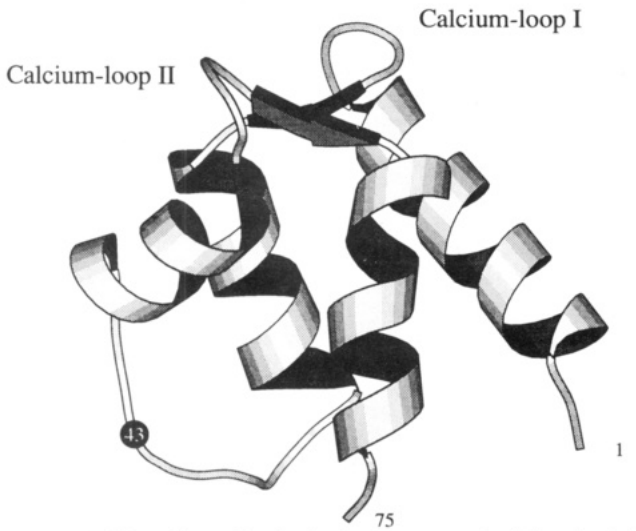

FIGURE 1: Three-dimensional solution structure of calcium-loaded calbindin D_{9k}. The ribbon diagram is based on the average structure of 27 solution structures calculated for calcium-loaded P43G calbindin D_{9k} (Kördel et al., 1992) and was generated using the program MOLSCRIPT (Kraulis, 1991). The helices are represented as coils, and the segments of the calcium-binding loops involved in the antiparallel β-type interaction are represented as broad arrows.

consequences of calcium binding in EF-hand calcium-binding proteins.

Calbindin D_{9k} has been selected as the initial subject for study because its small size (M_r 8500) makes it highly amenable to analysis by NMR spectroscopy. However, solutions of native and recombinant wild-type calbindin D_{9k} contain an equilibrium mixture of two isoforms due to proline cis–trans isomerism at the Gly42-Pro43 peptide bond (Chazin et al., 1989a; Kördel et al., 1990). Complete sequence-specific assignments have been made for both isoforms of the wild type and for the mutant calbindin D_{9k} with Pro43 substituted by glycine (Kördel et al., 1989, 1990). Conformational heterogeneity is eradicated in the mutant protein, and comparison of a variety of ^1H NMR parameters shows that only minute structural and dynamical differences exist between the mutant and wild-type proteins (Kördel et al., 1990). Since spectra of the mutant contain only one set of resonances, P43G is being used for all current NMR investigations.

The three-dimensional structure of calbindin D_{9k} has now been determined in solution, with and without calcium, using two-dimensional NMR spectroscopy (Akke et al., 1992; Kördel et al., 1992; N. J. Skelton, J. Kördel, and W. J. Chazin, unpublished results). These studies show that the structural differences between the two states are limited and are much smaller than what is predicted by the model based on the TnC crystal structure (Herzberg et al., 1986). In contrast, comparative analyses of dynamical information about the two states of calbindin D_{9k} from amide proton exchange rates, $^3J_{\alpha\beta}$ coupling constants, and estimated ring flip rates of Phe10 show a marked reduction in flexibility upon binding of calcium (Skelton et al., 1990; Akke et al., 1991; Skelton et al., 1992b). These results suggest that characterization of the changes in protein dynamics may be important for understanding the consequences of calcium binding.

Although a number of experimental techniques can characterize internal motions in proteins, NMR is potentially extremely useful because a large number of nuclear sites within a given molecule can be studied over a wide range of time scales (Brooks et al., 1988). For example, information about fast internal motions and overall rotational tumbling of a molecule can be obtained from ^{13}C and ^{15}N NMR relaxation measurements. The introduction of two-dimensional proton-detected heteronuclear techniques [reviewed by Bax et al. (1989)] has mitigated problems due to the inherent lack of sensitivity of ^{13}C and ^{15}N nuclei and the limited resolution of one-dimensional NMR techniques. Recently, investigations of NMR relaxation have been carried out for $^{13}C^{\alpha}$ nuclei at natural abundance in BPTI (Nirmala & Wagner, 1988) and a Xfin zinc finger (Palmer et al., 1991a), as well as for amide ^{15}N nuclei in uniformly enriched staphylococcal nuclease (Kay et al., 1989), interleukin-1β (Clore et al., 1990a), and the IIA domain of a glucose permease (Stone et al., 1992).

This paper reports on a study of the backbone dynamics of calcium-loaded calbindin D_{9k} based on ^{15}N relaxation measurements made by using proton detected ^{15}N–^1H 2D NMR spectroscopy. Sensitivity enhanced pulse sequences were utilized to halve the total time of acquisition required to achieve a given signal-to-noise ratio (Palmer et al., 1991b). The data for Ca^{2+}-loaded calbindin D_{9k} are compared with the available ^{15}N relaxation data for other proteins, with the amide proton exchange rates measured for Ca^{2+}-loaded calbindin D_{9k} (Skelton et al., 1992b), and with the dynamical information available from the *B*-factors of the X-ray crystal structure (Szebenyi & Moffat, 1986). In addition, the results reported here are used to differentiate regions in the NMR-derived solution structure of calcium-loaded calbindin D_{9k} that are poorly defined as a result of inherently high flexibility, from those with average flexibility but a low density of structural constraints. This study forms the background for a comparative analysis with the apo and half-saturated states of the protein, which will provide detailed information on the changes in dynamics that occur upon ion binding.

Materials and Methods

Sample Preparation. Uniformly ^{15}N-labeled P43G was produced on M9 minimal media containing $^{15}NH_4Cl$ as the sole nitrogen source as described in Skelton et al. (1992a). Protein was purified following the procedure described in Chazin et al. (1989b). All measurements were made on one 5 mM sample in 95% H_2O/5% D_2O, adjusted to pH 6.0 by addition of microliter quantities of 1 M HCl. To minimize the amount of dissolved oxygen in the NMR sample, all solvents and glassware were purged with argon prior to use, and the sample was prepared in an argon atmosphere. After the NMR tube was filled, the dead space over the sample solution was flushed with argon and the tube was shaken vigorously; this process was repeated four times. The NMR tube was flushed with argon one final time and then capped with a rubber septum (Wilmad) and sealed with parafilm.

Acquisition of NMR Spectra. Experiments were recorded at 300 K on Bruker AMX 500 (11.74 T) and AM 600 (14.10 T) spectrometers. The ^{15}N spin–lattice (R_1) and spin–spin (R_2) relaxation rate constants and steady-state $\{^1H\}$–^{15}N NOEs were measured from ^1H-detected ^1H–^{15}N correlation spectra recorded with sensitivity enhanced pulse sequences (Figure 2), whereby two orthogonal magnetization components are recorded simultaneously and subsequently deconvoluted to yield two pure phase data sets (Palmer et al., 1991b; N. J. Skelton, A. G. Palmer, M. Akke, J. Kördel, and W. J. Chazin, manuscript in preparation). For R_1 and R_2 measurements, the two data sets were added to yield a single spectrum with $\sqrt{2}$ higher signal-to-noise ratio than a conventional experiment acquired in the same time. The $\{^1H\}$–^{15}N NOEs were determined separately for each of the two data sets, which allowed two independent measurements of the NOE in the same time as a conventional experiment. The GARP-1 (Shaka et al., 1985) sequence was applied to saturate the protons during the re-

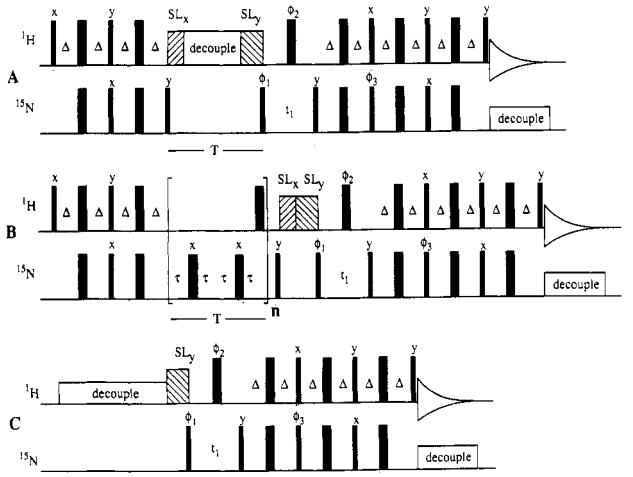

FIGURE 2: Sensitivity-enhanced pulse sequences for measurement of ^{15}N R_1 (A), R_2 (B), and $\{^1H\}$–^{15}N NOE (C) with ^1H detection. The phase cycling used for the R_1 and R_2 experiments is $\phi_1 = (x, -x, x, -x)$; $\phi_3 = (y, y, -y, -y)$; and receiver = $(x, -x, -x, x)$. The phase cycling used for the $\{^1H\}$–^{15}N NOE experiment is $\phi_1 = 8(x, -x)$; $\phi_2 = 2(y, y, y, y, -y, -y, -y, -y)$; $\phi_3 = 2(y, y, -y, -y), 2(-y, -y, y, y)$, and receiver = $2(x, -x, -x, x), 2(-x, x, x, -x)$. In all cases, each t_1 experiment is recorded twice with the phase of the 90° ^{15}N pulse immediately after t_1 increased by 180° between experiments. Linear combinations of these experiments enable the sensitivity enhancement method of Palmer et al. (1991b) to be employed. Quadrature detection in ω_1 can be achieved by the TPPI or the hypercomplex methods. The thin and thick vertical bars represent 90° and 180° radiofrequency pulses, respectively, and hatched vertical bars and SL denote spin–lock purge pulses. Pulses without phase designations are applied along the y-axis. Δ is set to $\sim 1/(4J_{NH})$. In sequences A and B, T was parametrically varied between 2D experiments.

covery period (T) of the R_1 experiments (Figure 2A), thereby eliminating effects on the ^{15}N longitudinal relaxation due to dipolar cross-relaxation and cross-correlation between dipolar and anisotropic chemical shift relaxation mechanisms (Boyd et al., 1990). A ^{15}N CPMG spin–echo sequence (Carr & Purcell, 1954; Meiboom & Gill, 1958) was applied during the transverse relaxation period (T) of the R_2 experiment (Figure 2B). The delay τ in Figure 2B was adjusted such that 2τ plus the ^{15}N 180° pulse length (80 μs) was equal to 1.0 ms; thus, the interval between the refocusing pulses was sufficiently short to effectively spin-lock the heteronuclear spins (Vold & Vold, 1976; Palmer et al., 1992). The effects of cross-correlation acting on ^{15}N transverse relaxation were suppressed by the application of ^1H 180° pulses in synchrony with the even echos in the ^{15}N CPMG sequence (Palmer et al., 1992; Kay et al., 1992). High-power ^{15}N pulses in the R_2 measurements were generated using an external amplifier (American Microwave Technology, Brea, CA; Model 3205). The duty cycle during the ^{15}N CPMG sequence was <10% to minimize contributions from $T_{2\rho}$ and sample heating. The GARP-1 scheme was used for ^1H saturation during the relaxation period in the $\{^1H\}$–^{15}N NOE experiments (Figure 2C).

All spectra were recorded with a spectral width of 12 500 Hz and 4096 real points in ω_2; digital oversampling by a factor of 2 reduces baseline distortions associated with the spectrometer's low-pass filters (Delsuc & Lallemand, 1986). Water suppression was achieved by the use of 0.5–1.5 ms spin–lock purge pulses (Messerle et al., 1989). The experiments at 11.74 T were recorded using time-proportional phase incrementation (TPPI) to obtain quadrature phase detection in ω_1 (Marion & Wüthrich, 1983); 300 real t_1 points were collected, which yielded a t_{1max} of 120 ms. The hypercomplex method was used to obtain quadrature phase detection in ω_1 (States et al., 1982) for spectra acquired at 14.10 T; 150 complex t_1 points were collected, which yielded a t_{1max} of 94 ms. For all of the experiments (Figure 2), the value of Δ for the INEPT polarization transfers (Morris & Freeman, 1979; Burum & Ernst, 1980) was set to 2.75 ms and decoupling of ^{15}N was performed using WALTZ-16 (Shaka et al., 1983). For the R_1 and R_2 measurements (parts A and B of Figure 2), the sums of the recycle delay and acquisition time in the sequences were set to 3.3 s (approximately 3 times the longest ^1H spin–lattice relaxation time) and the total numbers of transients recorded per t_1 point were 8 and 16 for real and complex data, respectively. For the $\{^1H\}$–^{15}N NOE measurements (Figure 2C), the ^1H recovery period prior to acquisition was 4.6 s (greater than 8 times the longest ^{15}N spin–lattice relaxation time) and the total numbers of transients recorded per t_1 point were 32 and 64 for real and complex data, respectively.

The R_1 values at 11.74 T were determined by recording 13 experiments using eight T delays [0.04 (×2), 0.13, 0.21, 0.41 (×2), 0.77, 1.23 (×2), 1.99 (×2), and 3.06 s (×2)] and at 14.10 T by recording nine experiments usign eight T delays [0.03 (×2), 0.13, 0.21, 0.41, 0.77, 1.23, 2.00, and 3.04 s]. A second series of nine R_1 experiments was recorded at 11.74 T using the conventional (as opposed to sensitivity enhanced) sequence with the same eight delay times and one duplicate of the shortest (0.04 s) delay. The R_2 values were determined at 11.74 T by recording 12 experiments with the seven delays [0.004 (×2), 0.032 (×2), 0.128 (×2), 0.220 (×2), 0.360, 0.800, and 1.3 s (×2)]. Four determinations of the NOEs were made at 11.74 T and at 14.10 T.

Data Processing. An in-house modified version of the FTNMR software (Hare Research Inc., Woodinville, WA) was utilized for data processing. All but two of the ^{15}N–^1H correlation peaks were well-resolved in the 2D spectrum; thus, a matched 6-Hz exponential filter could be applied in ω_2. Prior to Fourier transformation, the data were zero-filled once. In ω_1, the data were multiplied by a cosine bell function to minimize truncation artifacts and zero-filled to yield 1024 real data points in each column of the processed data. The first point in each row and column was halved before Fourier transformation to suppress ridges (Otting et al., 1985), and a low-pass filter was used to suppress the solvent signal in the time domain data (Marion et al., 1989). To further resolve the cross-peaks for Ser44 and Glu26, the data were reprocessed using a Lorentzian–Gaussian window function in ω_2 and the HSVD linear prediction algorithm (Barkhuijsen et al., 1987) was used to extend the ω_1 interferogram to 600 points. Details of the linear prediction analysis will be reported elsewhere (N. J. Skelton, A. G. Palmer, M. Akke, J. Kördel and W. J. Chazin, manuscript in preparation).

Analysis of Relaxation Rate Constants and NOEs. Intensities of the resonance peaks in the two-dimensional spectra were determined as the peak heights. The uncertainties in the measured peak heights (σ_h) were determined from duplicate spectra. The standard deviation of the differences between the heights of corresponding cross-peaks in pairs of spectra is equal to $\sqrt{2}\,\sigma_h$ under the assumption that the distributions of peak heights for different resonances are homoskedastic. The values of σ_h decreased for longer parametric delays but were always greater than the RMS baseplane noise. Values of σ_h were interpolated for those delays lacking a duplicate experiment. For the R_1 series at 14.70 T (and the conventional R_1 series at 11.74 T), the σ_h determined from duplicate experiments recorded at the shortest delay was used for all time points.

The experimental information obtained from inverse-detected relaxation measurements are formally identical to that

of the one-dimensional inversion recovery (Vold et al., 1968), CPMG (Meiboom & Gill, 1958), and steady-state {^{1}H}–^{15}N (Noggle & Schirmer, 1971) sequences. Relaxation rate constants were obtained from nonlinear fits of monoexponential equations for longitudinal and transverse relaxation using the Levenburg–Marquardt algorithm, as described previously (Palmer et al., 1991a). An offset parameter was introduced in the transverse relaxation equation (Vold & Vold, 1976). This parameter was statistically different from zero for only 10 of the 71 observable residues. The uncertainties in the values of R_1 and R_2 were determined as the formal standard deviations calculated from the covariance matrix in the nonlinear optimization routine. Steady-state NOEs were calculated as the ratios of the peak heights in the spectra recorded with and without proton saturation. The mean NOEs and standard deviations were calculated from the four independent measurements.

Calculation of Model-Free Parameters. The relaxation of an amide ^{15}N nucleus spin at high field strengths is dominated by the dipolar interaction with the directly attached proton and by the CSA mechanism (Abragam, 1961). The ^{15}N chemical shift tensor is approximately axially symmetric with a principal axis that is nearly colinear with the N–H bond; consequently, the relaxation parameters are functions of the spectral density function $J(\omega)$, given by the Fourier transform of the orientational correlation function for a unit vector along the nitrogen–hydrogen bond, at the five characteristic frequencies of a two-spin system (Kay et al., 1989). The apparent spin–lattice relaxation rate constant, ignoring cross-correlation effects, is the sum of the dipolar and CSA spin–lattice relaxation rate constants. The apparent spin–spin relaxation rate constant, ignoring cross-correlation effects, is the sum of the dipolar and the CSA spin–spin relaxation rate constants plus the rate constant (R_2^a) for other pseudo-first-order processes that contribute to the decay of transverse magnetization during the CPMG sequence (e.g., chemical exchange). Thus, the ^{15}N R_1 and R_2 relaxation rate constants and the NOEs are given by

$$R_1 = (d^2/4)[J(\omega_H - \omega_N) + 3J(\omega_N) + 6J(\omega_H + \omega_N)] + c^2J(\omega_N) \quad (1)$$

$$R_2 = (d^2/8)[4J(0) + J(\omega_H - \omega_N) + 3J(\omega_N) + 6J(\omega_H) + 6J(\omega_H + \omega_N)] + (c^2/6)[3J(\omega_N) + 4J(0)] + R_2^a \quad (2)$$

$$\text{NOE} = 1 + (d^2/4R_1)(\gamma_H/\gamma_N)[6J(\omega_H + \omega_N) - J(\omega_H - \omega_N)] \quad (3)$$

in which

$$d = (\mu_0 h/8\pi^2)\gamma_N\gamma_H\langle 1/r_{NH}^3\rangle \quad (4)$$

$$c = \omega_N(\sigma_\parallel - \sigma_\perp)/\sqrt{3} \quad (5)$$

and μ_0 is the permeability of free space, h is Planck's constant, γ_H and γ_N are the gyromagnetic ratios of ^{1}H and ^{15}N, respectively, r_{NH} is the nitrogen–proton bond length, ω_H and ω_N are the Larmor frequencies of ^{1}H and ^{15}N, and $\sigma_\parallel$ and $\sigma_\perp$ are the parallel and perpendicular components of the chemical shift tensor. The value of the chemical shift anisotropy ($\sigma_\parallel - \sigma_\perp$) for ^{15}N varies with the conformation of the polypeptide backbone (Shoji et al., 1989, 1990). Since calbindin D_{9k} is mainly helical (Szebenyi & Moffat, 1986; Kördel et al., 1989), a value of −160 ppm was used.

Available experimental data generally are insufficient to determine the spectral density functions explicitly; instead, the spectral density is modeled by a simpler function with fewer but physically meaningful parameters. The most common approach is the formalism of Lipari and Szabo (1982a,b), in which overall motion of the molecule is described by a single correlation time and the internal motions are described by two parameters: a generalized order parameter and an effective internal correlation time. Use of a single correlation time for overall motions assumes that the molecule can be modeled as a spherical rotor. The order parameter specifies the degree of spatial restriction of the bond vector. The square of the order parameter ranges from zero for isotropic motions to unity for completely restricted motions. However, the relationship between the order parameter and motional freedom is not monotonic; the order parameter can also be zero for certain restricted (nonisotropic) motions (cf. eq 7). The effective correlation time depends on both the amplitude and rate of the internal motion; hence, a specific motional model is needed for extracting the microscopic reorientation rate of the bond vector. The original model-free formalism has been extended to include separate motional processes on two different time scales (Clore et al., 1990b). Assuming that the overall and internal motions are independent and that the faster internal motion occurs on a time scale <10 ps, the corresponding spectral density function for the molecular motions is approximated by

$$J(\omega) = 2/5\left[\frac{S^2\tau_m}{1 + (\omega\tau_m)^2} + \frac{(S_f^2 - S^2)\tau}{1 + (\omega\tau)^2}\right] \quad (6)$$

in which $1/\tau = 1/\tau_m + 1/\tau_e$ and $S^2 = S_f^2S_s^2$, τ_m is the overall rotational correlation time of the molecule, S^2 is the square of the generalized order parameter, S_f^2 and S_s^2 are the squares of the order parameters for the motions on the fast and slow time scales, respectively, and τ_e is the effective correlation time for motions on the slower of the two time scales. For convenience, S^2, S_f^2, and S_s^2 are referred to simply as "order parameters" in the following discussion. If motional processes on the two time scales cannot be resolved, then eq 6 reduces to the original formalism by setting $S_f^2 = 1$. In this case, S^2 and τ_e are the generalized order parameter and effective correlation time for internal motions on a time scale faster than overall tumbling. Thus, when $S_f^2 = 1$, τ_e refers to motions on a different time scale than when $S_f^2 \neq 1$. A simple motional model casts fast internal motions as free diffusion within a cone of semiangle θ_o. Defining $\chi_o = \cos\theta_o$, the corresponding order parameter is given by (Lipari & Szabo, 1980, 1981)

$$S^2 = [1/2\chi_0(1 + \chi_0)]^2 \quad (7)$$

while the microscopic diffusion time constant (τ_D) can be extracted from

$$(1 - S^2)\tau_e = 6\tau_D[\chi_0^2(1 + \chi_0)^2\{\log[(1 + \chi_0)/2] + (1 - \chi_0)/2\}/[2(\chi_0 - 1)] + 1/24(1 - \chi_0)(6 + 8\chi_0 - \chi_0^2 - 12\chi_0^3 - 7\chi_0^4)] \quad (8)$$

The ratio of R_2/R_1 is a useful diagnostic parameter for initial evaluation of the relaxation data. As noted by Kay et al. (1989), the average value of R_2/R_1 for the backbone amides can be used to obtain an estimate of τ_m for the protein. In addition, if R_2/R_1 for a specific residue is much less than the average, internal motions contribute significantly to the relaxation; if R_2/R_1 is much greater than the average for a specific residue, R_2 contains significant contributions from R_2^a (eq 2). In the present context, the overall rotational correlation time and the individual internal motional parameters for each residue were determined simultaneously from the R_1, R_2, and NOE data by minimizing the sum of the squared residuals between the experimental data and relaxation parameters calculated using the model-free formalism (Palmer et al.,

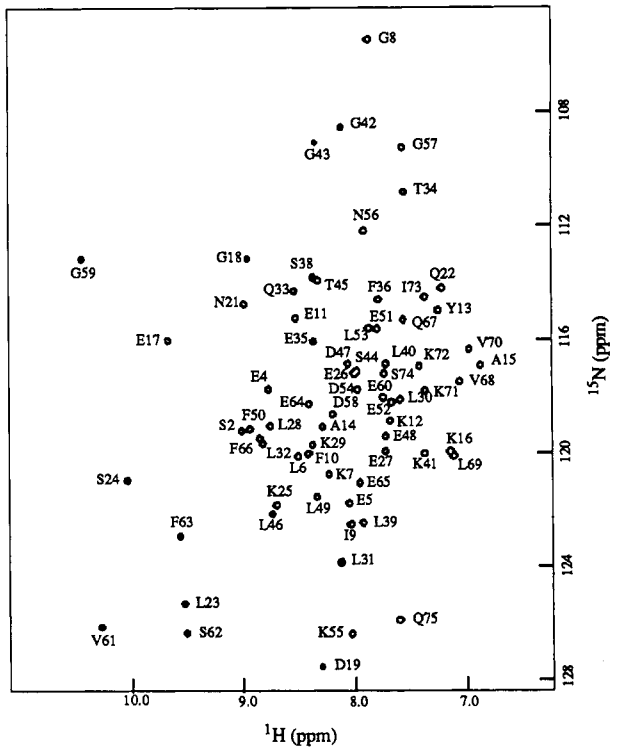

FIGURE 3: Double INEPT ^{15}N–^{1}H correlation spectrum of 5 mM calcium-loaded P43G calbindin D_{9k} at pH 6.0, 300 K, recorded with the pulse sequence in Figure 2B and $T = 0.004$ s. Each cross-peak is identified with the corresponding sequence-specific assignment.

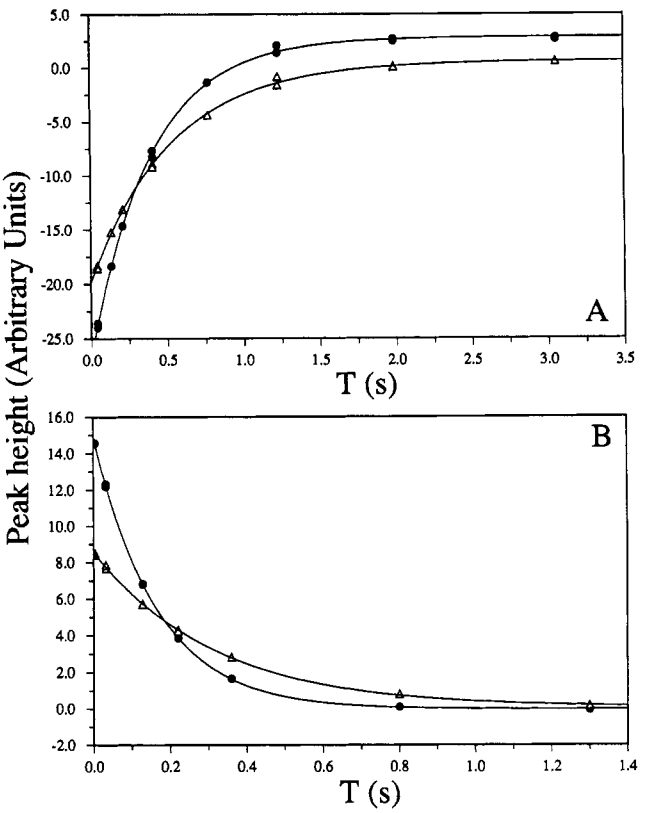

FIGURE 4: Typical relaxation decay curves for Leu28 (●) and Gly42 (△). Panel A shows the results for the inversion recovery R_1 measurements with use of the sequence of Figure 2A. Panel B shows the results for the CPMG R_2 measurements with use of the sequence of Figure 2B. The curves represent optimized monoexponential functions. Peak heights are given in arbitrary units with an uncertainty effectively smaller than the symbols, less than 0.24 unit in (A) and 0.06 unit in (B).

1991a). The model-free analysis was performed twice: first, τ_m, S^2, and τ_e were optimized with S_f^2 fixed at unity for all residues; second, the analysis was repeated with inclusion of S_f^2 in the spectral density function for those residues with R_2/R_1 more than one sample deviation below the average value. Initial estimates of S^2 (S_f^2 when necessary) and τ_e were obtained for each backbone amide by a grid search with τ_m fixed at the value obtained from the average R_2/R_1 ratio. Contributions to the R_2 values from decay processes other than dipolar and CSA relaxation were negligible; hence, the R_2^a term (eq 2) was not included in the calculations. The uncertainties given for the model free parameters in Tables II and III were estimated by Monte Carlo simulations as described by Palmer et al. (1991a); 300 simulated data sets were analyzed, and the uncertainties were taken as the standard deviations of the simulated model-free parameters.

RESULTS

Complete ^{15}N resonance assignments for calcium-loaded calbindin D_{9k} have been reported (Skelton et al., 1992a). Figure 3 shows a contour plot of a 2D ^{15}N–^{1}H correlation experiment recorded with the pulse sequence in Figure 2B and a delay time $T = 0.004$ s. The only cross-peak overlap is for Glu26 and Ser44 at $\omega_1 = 117.0$ ppm, $\omega_2 = 8.0$ ppm; however, these two signals are sufficiently resolved to allow reliable, albeit less precise, measurements of peak heights after resolution enhancement and linear prediction. Relaxation parameters were measured for the secondary backbone amides of all residues except Lys1. This resonance and that of the primary amine of Met0 are broadened beyond detection by solvent exchange under the conditions used in this study. Typical relaxation data and corresponding nonlinear fits are shown in Figure 4.

The calculated spin–lattice and spin–spin relaxation rate constants and the {^{1}H}–^{15}N NOEs are listed in Table I. The experimental R_1 values range from 1.47 to 2.61 s^{-1} at 11.74 T and from 1.41 to 2.24 s^{-1} at 14.10 T. If the residues with significantly smaller longitudinal relaxation rate constants (Lys41–Ser44, Ser74, and Gln75) are ignored, then the average and the sample deviations are 2.50 ± 0.09 s^{-1} and 2.15 ± 0.07 s^{-1} at 11.74 T and 14.10 T, respectively. The R_2 values range from 2.01 to 6.25 s^{-1} with the slowest transverse relaxation occurring for the same residues that exhibit the slowest longitudinal relaxation. Excluding these residues, the average R_2 value is 5.8 ± 0.3 s^{-1}. A negative NOE is observed only for Gln75, whereas the NOEs for all other residues span the range between 0.246 and 0.758 at 11.74 T and between 0.363 and 0.787 at 14.10 T. If the values for residues 41–44, 74, and 75 are discounted, a narrow distribution is observed for the NOEs (0.70 ± 0.05 at 11.74 T and 0.72 ± 0.04 at 14.10 T). As discussed elsewhere (N. J. Skelton, A. G. Palmer, M. Akke, J. Kördel, and W. J. Chazin, manuscript in preparation), the NOEs are not significantly biased by the effects of amide proton exchange or spin diffusion (Jelinski et al., 1980; Clore et al., 1990a; Smith et al., 1987). The small sample deviations from the mean R_2/R_1 and NOE values indicate that the relaxation properties are very similar for the majority of residues in the protein. The R_2/R_1 ratios at 11.74 T for each residue are given in Table I. The average ratio is 2.27 ± 0.18 and only Lys41, Gly42, Gly43, Ser44, Ser74, and Gln75 have R_2/R_1 ratios more than one standard deviation below the average. An estimate of τ_m (4.15 ± 0.04 ns) was obtained from the average R_2/R_1 ratio using eqs 1, 2, and 4–6.

The model-free parameters S^2 and τ_e are given in Table II for the analysis in which a second-order parameter (S_f^2) was included for residues Lys41–Ser44 and Ser74–Gln75. A plot of the generalized order parameters as a function of the amino

Table I: ^{15}N Relaxation Parameters for Calcium-Loaded P43G Calbindin D_{9k} at 300 K, pH 6.0

	11.74 T				14.1 T	
residue[a]	R_1 (s^{-1})	R_2 (s^{-1})	R_1/R_2[b]	NOE	R_1 (s^{-1})	NOE
Ser2	2.20 ± 0.03	4.73 ± 0.02	2.15 ± 0.04	0.553 ± 0.002	1.95 ± 0.04	0.596 ± 0.010
Glu4	2.36 ± 0.03	5.48 ± 0.02	2.32 ± 0.03	0.653 ± 0.001	2.00 ± 0.03	0.694 ± 0.025
Glu5	2.43 ± 0.03	5.47 ± 0.02	2.25 ± 0.04	0.637 ± 0.003	2.13 ± 0.04	0.662 ± 0.039
Leu6	2.48 ± 0.03	5.96 ± 0.02	2.41 ± 0.04	0.649 ± 0.003	2.12 ± 0.04	0.683 ± 0.032
Lys7	2.49 ± 0.03	5.95 ± 0.02	2.39 ± 0.04	0.704 ± 0.002	2.16 ± 0.03	0.737 ± 0.033
Gly8	2.52 ± 0.03	6.18 ± 0.02	2.46 ± 0.04	0.710 ± 0.003	2.16 ± 0.04	0.736 ± 0.036
Ile9	2.55 ± 0.03	5.83 ± 0.02	2.28 ± 0.04	0.710 ± 0.004	2.16 ± 0.04	0.729 ± 0.030
Phe10	2.58 ± 0.03	6.04 ± 0.02	2.34 ± 0.03	0.705 ± 0.003	2.21 ± 0.04	0.740 ± 0.032
Glu11	2.55 ± 0.03	6.13 ± 0.02	2.40 ± 0.04	0.718 ± 0.004	2.22 ± 0.04	0.746 ± 0.055
Lys12	2.52 ± 0.03	5.84 ± 0.02	2.32 ± 0.03	0.699 ± 0.002	2.18 ± 0.03	0.733 ± 0.046
Tyr13	2.49 ± 0.04	5.74 ± 0.02	2.31 ± 0.04	0.697 ± 0.002	2.14 ± 0.04	0.721 ± 0.027
Ala14	2.58 ± 0.03	6.07 ± 0.02	2.35 ± 0.03	0.714 ± 0.007	2.21 ± 0.03	0.732 ± 0.060
Ala15	2.53 ± 0.03	6.07 ± 0.02	2.40 ± 0.04	0.721 ± 0.005	2.17 ± 0.03	0.742 ± 0.028
Lys16	2.41 ± 0.02	5.51 ± 0.01	2.29 ± 0.03	0.687 ± 0.005	2.08 ± 0.03	0.726 ± 0.025
Glu17	2.47 ± 0.04	5.73 ± 0.02	2.31 ± 0.04	0.709 ± 0.001	2.10 ± 0.05	0.713 ± 0.035
Gly18	2.53 ± 0.05	5.85 ± 0.03	2.32 ± 0.06	0.737 ± 0.001	2.19 ± 0.06	0.734 ± 0.039
Asp19	2.27 ± 0.05	5.47 ± 0.03	2.41 ± 0.06	0.735 ± 0.003	1.96 ± 0.07	0.745 ± 0.015
Asn21	2.50 ± 0.04	5.93 ± 0.02	2.37 ± 0.05	0.717 ± 0.008	2.13 ± 0.04	0.739 ± 0.048
Gln22	2.48 ± 0.03	5.72 ± 0.02	2.31 ± 0.04	0.712 ± 0.002	2.13 ± 0.04	0.720 ± 0.026
Leu23	2.56 ± 0.05	5.78 ± 0.03	2.25 ± 0.05	0.716 ± 0.003	2.20 ± 0.06	0.740 ± 0.047
Ser24	2.54 ± 0.04	5.86 ± 0.03	2.31 ± 0.05	0.728 ± 0.002	2.18 ± 0.06	0.756 ± 0.021
Lys25	2.53 ± 0.03	5.93 ± 0.02	2.35 ± 0.03	0.732 ± 0.001	2.20 ± 0.04	0.734 ± 0.039
Glu26	2.49 ± 0.07	5.75 ± 0.13	2.31 ± 0.12	0.748 ± 0.008	2.19 ± 0.05	0.787 ± 0.017
Glu27	2.55 ± 0.04	6.02 ± 0.02	2.36 ± 0.04	0.728 ± 0.006	2.21 ± 0.05	0.743 ± 0.020
Leu28	2.57 ± 0.03	6.10 ± 0.02	2.37 ± 0.04	0.740 ± 0.003	2.19 ± 0.03	0.750 ± 0.041
Lys29	2.57 ± 0.03	6.15 ± 0.02	2.39 ± 0.03	0.716 ± 0.003	2.23 ± 0.04	0.729 ± 0.045
Leu30	2.56 ± 0.03	6.10 ± 0.02	2.39 ± 0.04	0.731 ± 0.005	2.16 ± 0.03	0.746 ± 0.041
Leu31	2.60 ± 0.03	6.11 ± 0.02	2.35 ± 0.04	0.727 ± 0.002	2.20 ± 0.03	0.753 ± 0.028
Leu32	2.61 ± 0.04	6.25 ± 0.02	2.39 ± 0.04	0.735 ± 0.004	2.24 ± 0.04	0.751 ± 0.027
Gln33	2.58 ± 0.03	5.96 ± 0.01	2.31 ± 0.03	0.711 ± 0.008	2.15 ± 0.03	0.736 ± 0.021
Thr34	2.52 ± 0.04	5.91 ± 0.03	2.34 ± 0.05	0.738 ± 0.002	2.19 ± 0.05	0.737 ± 0.043
Glu35	2.50 ± 0.05	6.00 ± 0.03	2.40 ± 0.06	0.724 ± 0.002	2.19 ± 0.06	0.731 ± 0.047
Phe36	2.41 ± 0.04	5.60 ± 0.02	2.32 ± 0.04	0.703 ± 0.005	2.02 ± 0.05	0.726 ± 0.034
Ser38	2.50 ± 0.04	5.72 ± 0.03	2.29 ± 0.05	0.721 ± 0.003	2.18 ± 0.05	0.722 ± 0.020
Leu39	2.54 ± 0.03	5.81 ± 0.02	2.29 ± 0.04	0.696 ± 0.004	2.21 ± 0.04	0.723 ± 0.026
Leu40	2.32 ± 0.03	4.94 ± 0.02	2.13 ± 0.04	0.560 ± 0.001	2.08 ± 0.05	0.606 ± 0.024
Lys41	2.13 ± 0.03	4.40 ± 0.01	2.07 ± 0.03	0.488 ± 0.005	1.89 ± 0.03	0.548 ± 0.010
Gly42	1.85 ± 0.03	3.14 ± 0.02	1.70 ± 0.04	0.246 ± 0.002	1.75 ± 0.04	0.363 ± 0.011
Gly43	1.92 ± 0.05	3.29 ± 0.03	1.71 ± 0.06	0.338 ± 0.005	1.81 ± 0.07	0.434 ± 0.010
Ser44	1.83 ± 0.09	3.54 ± 0.09	1.94 ± 0.14	0.429 ± 0.016	1.62 ± 0.06	0.698 ± 0.014
Thr45	2.21 ± 0.03	4.76 ± 0.02	2.16 ± 0.04	0.572 ± 0.002	1.95 ± 0.04	0.598 ± 0.027
Leu46	2.55 ± 0.03	5.63 ± 0.02	2.21 ± 0.04	0.715 ± 0.004	2.15 ± 0.05	0.732 ± 0.026
Asp47	2.44 ± 0.03	5.72 ± 0.01	2.35 ± 0.03	0.715 ± 0.003	2.14 ± 0.03	0.721 ± 0.040
Glu48	2.50 ± 0.03	5.74 ± 0.02	2.29 ± 0.03	0.710 ± 0.003	2.18 ± 0.04	0.723 ± 0.043
Leu49	2.52 ± 0.03	5.80 ± 0.02	2.30 ± 0.03	0.710 ± 0.001	2.21 ± 0.04	0.725 ± 0.016
Phe50	2.56 ± 0.03	5.96 ± 0.02	2.32 ± 0.03	0.726 ± 0.002	2.26 ± 0.04	0.731 ± 0.061
Glu51	2.60 ± 0.03	5.95 ± 0.02	2.29 ± 0.03	0.712 ± 0.007	2.22 ± 0.04	0.779 ± 0.023
Glu52	2.51 ± 0.03	5.79 ± 0.01	2.31 ± 0.03	0.691 ± 0.002	2.19 ± 0.03	0.717 ± 0.031
Leu53	2.55 ± 0.03	5.79 ± 0.02	2.28 ± 0.04	0.704 ± 0.003	2.16 ± 0.04	0.743 ± 0.014
Asp54	2.51 ± 0.03	5.90 ± 0.02	2.35 ± 0.04	0.719 ± 0.002	2.15 ± 0.03	0.749 ± 0.026
Lys55	2.34 ± 0.03	5.51 ± 0.01	2.36 ± 0.03	0.694 ± 0.006	1.98 ± 0.03	0.747 ± 0.035
Asn56	2.55 ± 0.03	5.86 ± 0.02	2.30 ± 0.04	0.719 ± 0.006	2.20 ± 0.04	0.726 ± 0.034
Gly57	2.44 ± 0.03	5.59 ± 0.02	2.29 ± 0.04	0.740 ± 0.002	2.11 ± 0.03	0.740 ± 0.023
Asp58	2.51 ± 0.04	6.05 ± 0.02	2.41 ± 0.04	0.758 ± 0.003	2.15 ± 0.04	0.750 ± 0.034
Gly59	2.57 ± 0.04	5.95 ± 0.03	2.31 ± 0.04	0.738 ± 0.003	2.21 ± 0.04	0.742 ± 0.028
Glu60	2.53 ± 0.03	5.85 ± 0.02	2.32 ± 0.04	0.721 ± 0.002	2.21 ± 0.04	0.735 ± 0.012
Val61	2.49 ± 0.04	5.51 ± 0.03	2.21 ± 0.05	0.708 ± 0.001	2.12 ± 0.06	0.727 ± 0.035
Ser62	2.58 ± 0.04	5.86 ± 0.03	2.27 ± 0.05	0.726 ± 0.002	2.22 ± 0.05	0.753 ± 0.014
Phe63	2.56 ± 0.04	5.96 ± 0.02	2.33 ± 0.04	0.731 ± 0.004	2.20 ± 0.05	0.763 ± 0.028
Glu64	2.44 ± 0.03	5.87 ± 0.02	2.41 ± 0.03	0.721 ± 0.003	2.12 ± 0.04	0.761 ± 0.032
Glu65	2.53 ± 0.04	6.00 ± 0.02	2.37 ± 0.04	0.718 ± 0.002	2.17 ± 0.04	0.744 ± 0.034
Phe66	2.58 ± 0.03	6.06 ± 0.02	2.35 ± 0.04	0.719 ± 0.002	2.20 ± 0.04	0.753 ± 0.050
Gln67	2.59 ± 0.03	5.91 ± 0.02	2.28 ± 0.04	0.698 ± 0.009	2.23 ± 0.03	0.715 ± 0.039
Val68	2.60 ± 0.03	6.11 ± 0.02	2.35 ± 0.03	0.699 ± 0.002	2.19 ± 0.04	0.732 ± 0.024
Leu69	2.55 ± 0.03	5.45 ± 0.01	2.14 ± 0.03	0.686 ± 0.004	2.20 ± 0.04	0.710 ± 0.035
Val70	2.49 ± 0.03	5.64 ± 0.02	2.27 ± 0.03	0.662 ± 0.004		
Lys71	2.47 ± 0.03	5.75 ± 0.01	2.32 ± 0.03	0.651 ± 0.003	2.16 ± 0.03	0.702 ± 0.018
Lys72	2.35 ± 0.03	5.23 ± 0.02	2.22 ± 0.04	0.589 ± 0.002	2.06 ± 0.03	0.621 ± 0.026
Ile73	2.28 ± 0.03	4.80 ± 0.01	2.10 ± 0.03	0.519 ± 0.01	2.02 ± 0.03	0.568 ± 0.026
Ser74	2.18 ± 0.03	4.23 ± 0.02	1.94 ± 0.03	0.460 ± 0.002	1.98 ± 0.04	0.524 ± 0.006
Gln75	1.74 ± 0.01	2.01 ± 0.00	1.37 ± 0.02	−0.344 ± 0.01	1.41 ± 0.02	−0.098 ± 0.010

[a] The resonances of Lys1 are broadened beyond detection at these conditions. Residues 3, 20, and 37 are prolines. Parameters for Val70 could not be accurately determined at 14.7 T due to interference from axial peaks. [b] Underlined R_1/R_2 ratios are more than one standard deviation lower than the average ratio.

Table II: Model-Free Parameters for Calcium-Loaded P43G Calbindin D_{9k} and Categorization According to Amide Proton Exchange Rates

residue	S^2 [a]	τ_e (ps)	k_{ex} categories[b]	residue	S^2 [a]	τ_e (ps)	k_{ex} categories[b]
Ser2	0.676 ± 0.055	48.1 ± 3.8	O	Lys41	0.548 ± 0.062	*	O
Glu4	0.787 ± 0.064	35.7 ± 2.9	⊗	Gly42	0.275 ± 0.031	*	O
Glu5	0.787 ± 0.064	43.9 ± 3.5	⊗	Gly43	0.306 ± 0.034	*	O
Leu6	0.854 ± 0.069	61.1 ± 4.8	⊗	Ser44	0.336 ± 0.036	*	O
Lys7	0.858 ± 0.069	18.7 ± 1.6	⊗	Thr45	0.683 ± 0.056	44.5 ± 3.7	O
Gly8	0.890 ± 0.072	20.0 ± 1.5	⊗	Leu46	0.816 ± 0.066	8.7 ± 0.5	⊗
Ile9	0.843 ± 0.068	13.6 ± 1.4	×	Asp47	0.827 ± 0.067	9.0 ± 0.8	⊗
Phe10	0.872 ± 0.070	20.8 ± 1.8	×	Glu48	0.831 ± 0.067	12.3 ± 1.1	⊗
Glu11	0.885 ± 0.071	10.8 ± 1.2	×	Leu49	0.839 ± 0.068	12.8 ± 1.1	×
Lys12	0.844 ± 0.069	20.7 ± 1.8	×	Phe50	0.863 ± 0.070	2.6 ± 0.5	×
Tyr13	0.829 ± 0.067	19.6 ± 1.7	×	Glu51	0.862 ± 0.070	13.1 ± 0.9	×
Ala14	0.878 ± 0.071	14.2 ± 1.2	×	Glu52	0.836 ± 0.068	25.0 ± 2.3	×
Ala15	0.877 ± 0.070	7.6 ± 0.9	×	Leu53	0.837 ± 0.068	16.3 ± 1.2	×
Lys16	0.795 ± 0.064	21.3 ± 1.8	×	Asp54	0.853 ± 0.069	7.5 ± 0.7	×
Glu17	0.828 ± 0.067	12.4 ± 1.1	×	Lys55	0.794 ± 0.064	16.4 ± 1.1	×
Gly18	0.849 ± 0.068	0.0 ± 0.1	⊗	Asn56	0.849 ± 0.068	9.2 ± 0.9	×
Asp19	0.789 ± 0.063	0.0 ± 0.1	⊗	Gly57	0.812 ± 0.066	0.0 ± 0.1	⊗
Asn21	0.856 ± 0.069	9.5 ± 0.5	×	Asp58	0.874 ± 0.071	0.0 ± 0.0	×
Gln22	0.828 ± 0.067	10.8 ± 0.8	×	Gly59	0.863 ± 0.070	0.0 ± 0.1	×
Leu23	0.838 ± 0.068	9.2 ± 0.7	×	Glu60	0.847 ± 0.068	6.7 ± 0.7	×
Ser24	0.850 ± 0.069	1.0 ± 0.2	×	Val61	0.800 ± 0.064	10.4 ± 0.8	×
Lys25	0.859 ± 0.069	0.0 ± 0.0	⊗	Ser62	0.850 ± 0.069	3.1 ± 0.4	×
Glu26	0.854 ± 0.070	0.0 ± 0.2	⊗	Phe63	0.864 ± 0.070	0.0 ± 0.2	⊗
Glu27	0.870 ± 0.070	3.8 ± 0.7	×	Glu64	0.848 ± 0.069	5.8 ± 0.4	⊗
Leu28	0.882 ± 0.071	0.0 ± 0.2	×	Glu65	0.867 ± 0.070	9.7 ± 0.6	×
Lys29	0.887 ± 0.072	13.5 ± 1.2	×	Phe66	0.876 ± 0.071	9.6 ± 0.9	×
Leu30	0.881 ± 0.071	0.0 ± 0.4	×	Gln67	0.855 ± 0.069	27.1 ± 3.4	×
Leu31	0.884 ± 0.072	2.4 ± 0.4	×	Val68	0.881 ± 0.071	28.4 ± 2.5	×
Leu32	0.903 ± 0.073	0.0 ± 0.0	×	Leu69	0.789 ± 0.064	21.2 ± 1.9	×
Gln33	0.861 ± 0.070	16.3 ± 1.1	×	Val70	0.812 ± 0.066	37.0 ± 3.1	×
Thr34	0.856 ± 0.069	0.0 ± 0.0	×	Lys71	0.826 ± 0.067	48.0 ± 4.0	⊗
Glu35	0.867 ± 0.070	4.9 ± 0.4	×	Lys72	0.749 ± 0.061	55.1 ± 4.4	⊗
Phe36	0.808 ± 0.065	14.3 ± 1.3	×	Ile73	0.683 ± 0.056	61.1 ± 5.0	O
Ser38	0.830 ± 0.067	5.9 ± 0.6	⊗	Ser74	0.488 ± 0.056	*	O
Leu39	0.840 ± 0.068	22.4 ± 2.0	⊗	Gln75	0.096 ± 0.011	*	O
Leu40	0.706 ± 0.057	53.6 ± 4.3	O				

[a] Generalized order parameter $S^2 = S_f^2 S_s^2$ for all but the underlined residues, for which $S_f^2 = 1$ and $S^2 = S_s^2$. [b] Symbols: O, $k_{ex} > 0.01$ s^{-1} and $S^2 < 0.75$; ⊗, $k_{ex} > 0.01$ s^{-1} and $S^2 > 0.75$; ×, $k_{ex} < 0.01$ s^{-1} and $S^2 > 0.75$; *, residues where S_f^2 was included as a model-free parameter, the effective correlation time (τ_e) for the fast internal motions was assumed to be <10 ps.

Table III: Extended Model-Free Parameters for Calcium-Loaded P43G Calbindin D_{9k}

residue	S_f^2	S_s^2	τ_e (ps)
Lys41	0.783 ± 0.064	0.700 ± 0.055	1454.2 ± 131.8
Gly42	0.723 ± 0.059	0.380 ± 0.029	1657.4 ± 138.7
Gly43	0.713 ± 0.059	0.428 ± 0.032	1816.1 ± 157.3
Ser44	0.660 ± 0.055	0.509 ± 0.035	2686.9 ± 239.8
Ser74	0.790 ± 0.064	0.618 ± 0.050	1723.1 ± 141.5
Gln75	0.678 ± 0.055	0.141 ± 0.012	1166.5 ± 94.4

acid sequence is shown in Figure 5A. Table III contains the S_f^2, S_s^2, and τ_e values for Lys41–Ser44 and Ser74–Gln75. Inclusion of S_f^2 in the extended model-free formalism resulted in 3–50-fold reductions in the sum of the squared residuals for these residues. The generalized order parameters for Lys41–Ser44 and Ser74–Gln75 were an average of 0.16 ± 0.04 unit smaller when S_f^2 was included in the model-free formalism than when S_f^2 was fixed at unity. The optimized global value of τ_m was determined to be 4.25 ± 0.04 ns, in good agreement with the value calculated from the R_2/R_1 ratios. The convergence of the optimization procedure can be judged by comparing the experimentally measured relaxation parameters with those predicted by the model-free parameters. The mean value of the sum of the squared residuals per residue, averaged over the entire sequence, was 13.7; therefore, on average, experimental and calculated relaxation values agreed to within less than 1.5 times the experimental uncertainties. Alternatively, the RMS differences between the experimental and calculated relaxation parameters were 0.06 s^{-1} (~2.5%) at 11.74 T and 0.09 s^{-1} (~4.3%) at 14.10 T for R_1, 0.02 s^{-1} (~0.4%) for R_2, and 0.01 (~1.7%) at 11.74 T and 0.03 (~4.0%) at 14.10 T for the NOE. These results demonstrate that the formalism employed herein accurately describes the relaxation data.

In Table IV, model-free parameters are grouped according to the elements of regular secondary structure of calbindin D_{9k} identified in solution (Kördel et al., 1990). The cone semiangles and internal diffusion time constants for the motional model for precession in a cone (eqs 7 and 8) are also reported in Table IV. ANOVA (Devore, 1982) indicates that the average order parameters (and cone semiangles) for the helices and calcium-binding loops are statistically indistinguishable at the 95% confidence level; however, ANOVA and Scheffe multiple comparisons (Devore, 1982) indicate that the average effective correlation times (and the internal diffusion time constants) for helices I and IV are longer than for helices II and III or for the calcium-binding loops.

Discussion

The ^{15}N relaxation parameters measured for calcium-loaded calbindin D_{9k} show that the linker loop and a few residues at the N- and C-termini are more flexible than the two EF-hands. No significant differences are observed between the order parameters for individual α-helices or for the two different calcium-binding loops. Furthermore, the calcium-binding loops and the helices have similar average S^2 values of 0.85 ± 0.04 and 0.83 ± 0.03, respectively; interestingly, the effective correlation times for helices I and IV appear to be longer than for helices II and III or for the calcium-binding loops. The linker region joining the two subdomains of the molecule does have significantly higher flexibility as judged from the lower

Table IV: Average Model-Free Parameters and the Corresponding Cone Semiangles and Diffusion Time Constants for the Different Secondary Structure Elements in Calcium-Loaded P43G Calbindin D_{9k}

structure element	residues	S^2	τ_e (ps)	θ_0[a] (deg)	τ_D[b] (ps)
helix I	Glu4–Ala15	0.850 ± 0.035	23.9 ± 15.5	18.6 ± 2.3	129 ± 77
Ca^{2+}-loop I	Lys16–Ser24	0.829 ± 0.025	8.0 ± 7.4	20.0 ± 1.6	38 ± 32
helix II	Lys25–Glu35	0.873 ± 0.015	3.7 ± 5.8	17.1 ± 1.1	24 ± 38
linker loop	Phe36–Thr45	**0.592 ± 0.233**	**860 ± 1000**[c]	*	*
helix III	Leu46–Asp54	0.840 ± 0.016	11.9 ± 6.3	19.3 ± 1.0	61 ± 32
Ca^{2+}-loop II	Lys55–Ser62	0.836 ± 0.030	5.7 ± 6.0	19.6 ± 1.9	26 ± 26
helix IV	Phe63–Ile73	0.823 ± 0.061	27.5 ± 20.7	20.3 ± 3.7	120 ± 74

[a] Cone semiangles and diffusion time constants are not calculated for the linker loop since it contains residues for which two order parameters are needed to describe the relaxation data (indicated by an asterisk). Average cone semiangles calculated from S^2 using eq 7. [b] Average diffusion time constant calculated from S^2 and τ_e using eq 8. [c] Average τ_e for motions in the slower of two distinct time scales.

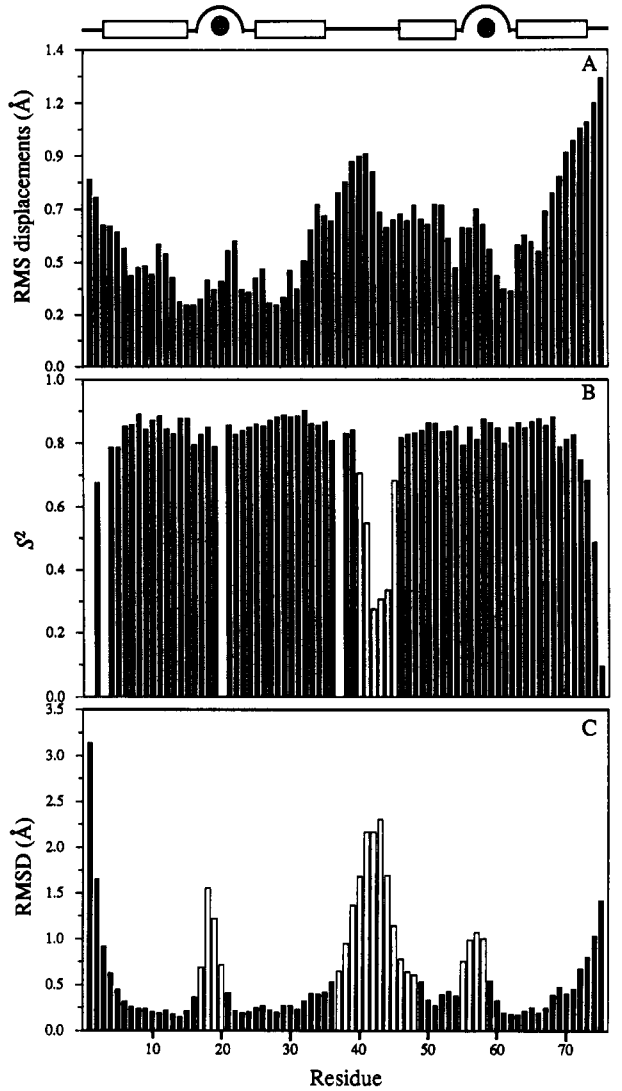

FIGURE 5: Comparison of structural and dynamic parameters of the backbone amide nitrogens of calcium-loaded bovine calbindin D_{9k}: (A) crystallographic RMS displacements (Szebenyi & Moffat, 1986); (B) order parameters from the ^{15}N relaxation studies; (C) average RMS deviations of the refined solution structures from the mean structure (Kördel et al., 1992). The elements of regular secondary structure are identified above the diagram with the α-helices indicated by rectangular boxes, the calcium-binding loops by semicircular arcs, and the Ca^{2+} ions by filled circles. Disregarding the termini, order parameters in (B) smaller than 0.75 and RMSD values in (C) larger than 0.6 Å are indicated with open bars.

average S^2 value of 0.59 ± 0.23 and the apparent existence of motions on multiple time scales. The magnitude of the order parameters in calcium-loaded calbindin D_{9k} is in good agreement with those found in previous studies of backbone ^{15}N dynamics. The average S^2 values in staphylococcal nuclease are reported to be 0.86 for residues in α-helix (±0.03) as well as β-sheet (±0.04), turns (±0.04), and one of the loops (±0.04) (Kay et al., 1989). The S^2 values for interleukin-1β have not been grouped according to secondary structure elements, but the overall average value of S^2 was found to be 0.82 ± 0.05 (Clore et al., 1990a). The average value of S^2 for the β-sheet structures of the IIa domain of a glucose permease is 0.81 ± 0.06 (Stone et al., 1992). The values of S^2 for the $^{13}C^{\alpha}$ atoms in the X-fin zinc finger [0.89 ± 0.05 for the structurally ordered part of the molecule (Palmer et al., 1991a)] is in good agreement with the ^{15}N backbone amide values found for calcium-loaded calbindin D_{9k} as well as interleukin-1β, staphylococcal nuclease, and the glucose permase IIa domain.

The ratios of the three principal moments of inertia for the protonated crystal structure (Szebenyi & Moffat, 1986) are 1.00:1.01:1.21, which would indicate that the global shape of calbindin D_{9k} is very well approximated by a sphere. Assuming that the partial volume of calbindin D_{9k} is 0.72 cm^3/g and that the surface hydration is 0.35 g of H_2O/g of protein, a values of τ_m = 3.1 ns for calbindin D_{9k} is calculated from the Stokes–Einstein relation (Cantor & Schimmel, 1980). Rotational correlation times for calbindin D_{9k} of 2 ns and 4.2 ± 0.7 ns have been reported as measured by ^{43}Ca NMR relaxation measurements (Vogel et al., 1985) and fluorescence depolarization of the Tyr13 ring (Rigler et al., 1990), respectively. The value of 4.25 ± 0.04 ns determined from the ^{15}N relaxation parameters agrees well with these other values.

Interpretation of Model-Free Parameters. The generalized order parameter commonly is interpreted as a measure of the geometrical restriction of the N–H bond vectors. Although, even for simple motional models (e.g., eq 7), the relationship between S^2 and the amplitude of internal motions is not monotonic, such an interpretation generally is useful. For relatively highly restricted backbone librational motions, cone semiangles subtended by the bond vectors, calculated by eq 7, provide additional approximate indications of the physical amplitudes of the motions (Table IV). The physical interpretation and significance of order parameters calculated for motions on different time scales (S_f^2 and S_s^2) are less well established. Previous studies (Clore et al., 1990a,b) have interpreted S_f^2 using a model for diffusion in a cone and S_s^2 using a jump model. In the present instance, the mathematical improvement in the optimization for residues Lys41–Ser44 and Ser74–Gln75 upon addition of the parameter S_f^2 does not establish that the corresponding spectral density functions are more physically realistic than alternative models that incorporate higher moments (Lipari & Szabo, 1982a) or distributions (Fedatov et al., 1987; Zang et al., 1990) of the time constants for internal motions. As these alternative extensions to the simple model-free formalism yield very different physical insights, the results for Lys41–Ser44 and Ser74–Gln75 have not been interpreted further.

Effective correlation times are more difficult to interpret than generalized order parameters because, as given specifi-

cally for diffusion in a cone by eq 8, τ_e generally depends on both the rate and amplitudes of the internal motions. Consequently, as shown in Table IV, microscopic time constants calculated for a particular model can differ substantially from the original values of τ_e. In addition, possible contributions to the internal correlation function from extremely fast, subpicosecond, motions observed in molecular dynamics simulations (Olejniczak et al., 1984; Kördel & Teleman, 1992) further complicate interpretation of τ_e. Nonetheless, the observation that the average values of τ_e and τ_D for helices I and IV differed significantly from the values for helices II and III and the calcium-binding loops is particularly noteworthy because no corresponding differences were observed for the order parameters. Thus, the microscopic rates of internal motions, or their relative distributions, may be different for N–H bond vectors in helcies I and IV than in other regular structural elements, even though the degree of geometrical restriction is similar. Measurements of relaxation parameters for backbone $^{13}C^{\alpha}$ nuclei are in progress to confirm this observation.

Correlation with Crystallographic B-Factors. Structural studies using X-ray crystallography are averaged over the time required to collect the data (a minimum of at least several hours) as well as over the statistical variability of the molecules in the crystal(s). Although information on the time scale of these variations cannot be obtained, the random displacements of the atoms are manifested as an increased width of the electron density peaks and can be characterized by Debye–Waller (or temperature) factors (B). Assuming the simple case of isotropic, harmonic displacements, the B-factor is related to the mean square atomic displacement ($\langle \Delta r^2 \rangle$) by (Willis & Pryor, 1975)

$$\langle \Delta r^2 \rangle = 3B/8\pi^2 \qquad (9)$$

Although the spatial displacements have contributions from lattice disorder as well as thermal motion (conformational and vibrational fluctuations), the mean square atomic displacements of the backbone nitrogens in the crystal structure can be compared with the NMR-derived order parameters in solution [e.g., Clore et al. (1990a)]. The $\langle \Delta r^2 \rangle$ from the crystal structure of calbindin D_{9k} (Szebenyi & Moffat, 1986) and the S^2 values determined here are plotted versus residue number in panels A and B of Figure 5, respectively. Increased mobility is observed in the N- and C-termini, the N-terminal region of helix I, the C-terminal region of helix IV, and the central linker region joining the two EF-hands, as evidenced by both lower order parameters and higher B-factors. The value of the linear correlation coefficient between $\langle \Delta r^2 \rangle$ and S^2 is –0.6.

In the two previously published ^{15}N studies of protein backbone dynamics, Kay et al. (1989) reported that no correlation was apparent between the temperature factors and order parameters for staphylococcal nuclease, whereas Clore et al. (1990a) reported some correlation in general for interleukin-1β, but with a number of specific exceptions. In contrast, the present results show a rather good correlation between order parameters and B-factors. The discrepancies may arise because the B-factor is sensitive to both fast and slow time-scale dynamics, whereas S^2 is a function of rapid motions only (Kay et al., 1989). However, considering the large number of uncertainties in comparing order parameters and B-factors, a more substantial database of results is required before conclusive statements can be made.

Conformational Heterogeneity in Native Folded Calbindin D_{9k}. At ambient temperatures, the peptide bond between Gly42 and Pro43 in native and recombinant wild-type calbindin D_{9k} undergoes cis–trans interconversion in solution (Chazin et al., 1989a). This conformational heterogeneity does not affect the global structure of the protein and, in fact, the measured cis–trans exchange rate in the folded protein is comparable to that of small model peptides (Kördel et al., 1990). These observations suggest that this region of the linker loop between the two EF-hands is highly flexible. This hypothesis is confirmed by the low order parameters for residues Leu40–Thr45. However, the site of the Pro43 → Gly mutation is at the center of this flexible loop; therefore, the loss of conformational restraint upon substitution of the most conformationally restrictive amino acid, proline, with the least conformationally restrictive amino acid, glycine, may contribute to the high flexibility observed in this region. ^{15}N relaxation measurements for the wild-type protein are currently in progress to verify that the backbone dynamics in the linker loop are not significantly affected by the Pro43 → Gly mutation.

The crystal structure of wild-type calbindin D_{9k} has recently been determined at 1.6-Å resolution (Svensson et al., 1992). In this new structure, conformational heterogeneity in the Lys41–Pro43 segment of the linker loop has been modeled as a 50/50 mixture of molecules with the Gly42–Pro43 peptide bond in cis and trans conformation, respectively. The B-factors remain elevated in the linker loop even after modeling cis–trans isomerization as a form of static disorder. In absolute numbers, the B-factors are comparable to those obtained in the 2.3-Å structure of native bovine calbindin D_{9k} modeled with only trans-Pro43 (Szebenyi & Moffat, 1986). The order parameters in the linker region imply that the high B-factors observed in the crystal structures are primarily the result of flexibility in the loop rather than static disorder.

Comparison to Hydrogen Exchange Rates. The exchange of the backbone amide protons with solvent is an alternative method to obtain information about the dynamic properties of proteins. Regardless of the mechanism by which the amide proton exchange occurs, the frequency of the opening motions which lead to exchange must be equal to (EX_1 mechanism) or faster than (EX_2 mechanism) the observed rate of amide proton exchange. The backbone amide proton exchange rates of calbindin D_{9k} span the range 10^{-8}–10 s^{-1} at pH 6.0 and 300 K (Skelton et al., 1992b); under these experimental conditions, the motional processes governing amide proton exchange are expected to be significantly slower than the motions to which ^{15}N relaxation parameters are sensitive (Wagner, 1983; Roder et al., 1985).

In calcium-loaded calbindin D_{9k}, three distinct categories are found for the correlation between the backbone order parameters and the amide hydrogen exchange rates (see Table II): (i) slow exchange with solvent ($k_{ex} < 0.01$ s^{-1}) and high order parameters ($S^2 > 0.75$); (ii) rapid exchange with solvent ($k_{ex} > 0.01$ s^{-1}) and low order parameters ($S^2 < 0.75$) (iii) rapid exchange with solvent but high order parameters. As might be expected, residues with slow amide proton exchange rates and low order parameters are not observed.

The correlation between high values of S^2 and slow amide proton exchange in category i indicates that portions of the protein are relatively immobile over a wide range of time scales; conversely, the correlation between low values of S^2 and rapid amide proton exchange in category ii indicates that other regions of the protein are relatively mobile over a wide range of time scales. All of the residues in category i are located in the helices or calcium-binding loops and have amide protons that are involved in intramolecular hydrogen bonds in the crystal structure (Szebenyi & Moffat, 1986). Category ii consists of Ser2 near the N-terminus of the protein, Ile73–Gln75 in helix IV at the C-terminus of the protein, plus five

consecutive residues in the linker loop (Leu40–Thr45). None of the amide protons of these residues are involved in well-formed, stable hydrogen bonds in the crystal structure. Although the amide protons of Ile73–Gln75 have each been assigned to specific intramolecular helical hydrogen bonds, these three residues have the highest average main-chain *B*-factors in the protein. Two "possible" hydrogen bonds, which do not completely satisfy standard hydrogen-bond criteria, have been assigned for the amide protons of Thr45 and Gln75. In summary, a good correlation between the picosecond to nanosecond motions governing relaxation and the slower motions that lead to solvent access to the amide proton, and hence exchange, is observed for the residues in categories i and ii.

The high backbone ^{15}N order parameters and fast amide proton exchange observed for category iii demonstrate that portions of the protein can be rigid on a fast (picosecond to nanosecond) time scale, yet relatively mobile on a slower time scale. Category iii consists of two residues (Lys71–Lys72) adjacent to a flexible C-terminal segment in category ii, residues at the N-terminus of each of the four helices (Glu4–Glu8, Lys25–Glu26, Leu46–Glu48, Phe63–Glu64), Ser38–Leu39 in the linker loop, and three residues in the calcium-binding loops (Gly18, Asp19, Gly57). Despite the high order parameters for all of these residues, only Leu6, Lys7, Leu39, and Lys72 are assigned specific intramolecular hydrogen bonds, and Glu5, Gly8, Glu48, Gly57, and Lys71 are assigned "possible" hydrogen bonds, in the crystal structure. These observations demonstrate that a high order parameter for an N–H vector is not a reliable means for identifying intramolecular hydrogen bonds and that hydrogen bonding is only one of the mechanisms by which the mobility of the backbone is reduced on the picosecond to nanosecond time scale.

The correlation between the backbone order parameters and the hydrogen exchange rates in categories i and ii suggests that high flexibility (low order parameters) on the picosecond to nanosecond time scale results in a higher propensity for flexibility at the slower amide proton exchange time scale. However, the combination of high values of S^2 and rapid amide proton exchange for the residues in category iii demonstrate that the motional processes governing ^{15}N relaxation and amide proton exchange are not invariably correlated; the rate of fluctuations that lead to fast amide proton exchange are not always reflected in the relative magnitudes of the ^{15}N relaxation parameters. The observations reported here highlight the complementarity of the two techniques and demonstrate that a complete survey of protein internal dynamics requires a combination of experimental methods.

Correlation of Low Order Parameters with Poor Structural Definition. A high-resolution solution structure of calcium-loaded P43G calbindin D_{9k} has recently been determined by NMR spectroscopy (Kördel et al., 1992). Comparison of the number of NOE constraints with the average RMS deviations of the solution structures shows a distinct correlation between the number of constraints per residue and the degree of definition of the structures (Kördel et al., 1992). The helices are well defined with an average of 32 constraints per residue whereas the termini, linker region, and calcium-binding loops all have much fewer constraints and poorer definition. Plots of S^2 and local RMS deviation versus residue number are shown in panels B and C of Figure 5, respectively. The N- and C-termini and the linker region have low order parameters (and high *B*-factors, Figure 5A); consequently, the high RMSD values observed in the solution structures reflect conformational disorder in these regions of the protein. In contrast, the calcium-binding loops have order parameters similar to those of the helices; therefore, the structural uncertainty for these regions in the solution structure is a by-product not of high mobility but rather of geometrical factors or spectral degeneracies that limit the number of observable NOE cross-peaks for residues in the calcium-binding loop regions.

These conclusions are also supported by two sets of experimental observations that are sensitive to protein dynamics at slower time scales than τ_m. First, the observation of a single set of resonances, the lack of exchange cross-peaks in NOESY spectra, and the absence of incommensurate NOEs indicate that calbindin D_{9k} largely occupies a single time-averaged conformation on the millisecond to second time scale. Second, the absence of observable exchange broadening as judged from the R_2/R_1 ratios in Table II indicates that no exchange processes occur on a time scale faster than 1 ms, the delay used between the 180° pulses in the CPMG sequence (Kay et al., 1989). The cumulative evidence showing that structural uncertainty in the calcium-binding loops is not due to high mobility has stimulated further investigations in our laboratory to obtain additional structural constraints from multidimensional heteronuclear NMR experiments, in order to more clearly define the structure of the calcium-binding loop regions in solution.

The ^{15}N relaxation parameters measured for calcium-loaded calbindin D_{9k} constitute the first part of a comparative analysis of the dynamics of the protein with different levels of calcium loading. The goals of this research program are to assess the extent to which calcium binding affects the flexibility of the core and the loops of the protein. Parallel studies of structure and dynamics will yield detailed information about the molecular mechanisms of calcium binding and cooperativity in calbindin D_{9k} and should provide important insights for other members of the calmodulin superfamily of calcium-binding proteins.

Acknowledgments

We gratefully acknowledge Professor Sture Forsén for his encouragement, helpful discussions, and guidance; Dr. Mark Rance for continued assistance with experimental technique; Eva Thulin for protein expression and purification; Drs. Anders Svensson, Wayne Fairbrother, and Martin Stone for making data available prior to publication and for stimulating discussions; Dr. Ad Bax for sending a preprint of a manuscript; and Beth Larson for assistance with preparation of the manuscript.

References

Abragam, A. (1961) *The Principles of Nuclear Magnetism*, Clarendon Press, Oxford, England.

Akke, M., Forsén, S., & Chazin, W. J. (1991) *J. Mol. Biol. 220*, 173–189.

Akke, M., Drakenberg, T., & Chazin, W. J. (1992) *Biochemistry 31*, 1011–1020.

Barkhuijsen, H., Beer, R. J., & Van Ormondt, D. (1987) *J. Magn. Reson. 73*, 553–557.

Bax, A., Sparks, S. W., & Torchia, D. A. (1989) *Methods Enzymol. 176*, 134–150.

Boyd, J., Hommel, U., & Campbell, I. D. (1990) *Chem. Phys. Lett. 175*, 477–482.

Brooks, C. L., III., Karplus, M., & Pettitt, B. M. (1988) *Proteins: A Theoretical Perspective of Dynamics, Structure, and Thermodyanmics*, J. Wiley & Sons, New York.

Burum, D. P., & Ernst, R. R. (1980) *J. Magn. Reson. 39*, 163–168.

Cantor, R. C., & Schimmel, P. R. (1980) *Biophysical Chemistry*, Part II, p 461, W.H. Freeman, San Francisco.
Carr, H. Y., & Purcell, E. M. (1954) *Phys. Rev. 94*, 630–638.
Chazin, W. J., Kördel, J., Drakenberg, T., Thulin, E., Brodin, P., Grundström, T., & Forsén, S. (1989a) *Proc. Natl. Acad. Sci. U.S.A. 86*, 2195–2198.
Chazin, W. J., Kördel, J., Drakenberg, T., Thulin, E., Hoffmann, T., & Forsén, S. (1989b) *Biochemistry 28*, 8646–8653.
Clore, G. M., Driscoll, P. C., Wingfield, P. T., & Gronenborn, A. M. (1990a) *Biochemistry 29*, 7387–7401.
Clore, G. M., Szabo, A., Bax, A., Kay, L. E., Driscoll, P. C., & Gronenborn, A. M. (1990b) *J. Am. Chem. Soc. 112*, 4989–4991.
Delsuc, M. A., & Lallemand, J. Y. (1986) *J. Magn. Reson. 69*, 504–507.
Devore, J. L. (1982) *Probability and Statistics for Engineering and the Sciences*, Brooks/Cole, Monterey, CA.
Fedatov, V. D., & Kivayeva, L. S. (1987) *J. Biomol. Struct. Dyn. 4*, 599–619.
Herzberg, O., Moult, J., & James, M. N. G. (1986) *J. Biol. Chem. 261*, 2638–2644.
Jelinski, L. W., Sullivan, C. E., & Torchia, D. A. (1980) *J. Magn. Reson. 41*, 133–139.
Kay, L. E., Torchia, D. A., & Bax, A. (1989) *Biochemistry 28*, 8972–8979.
Kay, L. E., Nicholson, L. K., Delagio, F., Bax, A., & Torchia, D. A. (1992) *J. Magn. Reson. 97*, 359–375.
Kördel, J. & Teleman, O. (1992) *J. Am. Chem. Soc.* (submitted for publication).
Kördel, J., Forsén, S., & Chazin, W. J. (1989) *Biochemistry 28*, 7065–7074.
Kördel, J., Forsén, S., Drakenberg, T., & Chazin, W. J. (1990) *Biochemistry 29*, 4000–4009.
Kördel, J., Skelton, N. J., Akke, M., & Chazin, W. J. (1992) *J. Mol. Biol.* (submitted for publication).
Kraulis, P. (1991) *J. Appl. Crystallogr. 24*, 946–950.
Kretsinger, R. H. (1987) *Cold Spring Harbor Symp. Quant. Biol. 52*, 499–510.
Linse, S., Brodin, P., Drakenberg, T., Thulin, E., Sellers, P., Elmdén, K., Grundström, T., & Forsén, S. (1987) *Biochemistry 26*, 6723–6735.
Lipari, G., & Szabo, A. (1980) *Biophys. J. 30*, 489–506.
Lipari, G., & Szabo, A. (1981) *J. Chem. Phys. 75*, 2971–2976.
Lipari, G., & Szabo, A. (1982a) *J. Am. Chem. Soc. 104*, 4546–4559.
Lipari, G., & Szabo, A. (1982b) *J. Am. Chem. Soc. 104*, 4559–4570.
Manalan, A. S., & Klee, C. B. (1984) *Adv. Cyclic Nucleotide Protein Phosphorylation Res. 18*, 227–278.
Marion, D., & Wüthrich, K. (1983) *Biochem. Biophys. Res. Commun. 113*, 967–974.
Marion, D., Ikura, M., & Bax, A. (1989) *J. Magn. Reson. 84*, 425–430.
Meiboom, S., & Gill, D. (1958) *Rev. Sci. Instrum. 29*, 688–691.
Messerle, B. A., Wilder, G., Otting, G., Weber, C., & Wuthrich, K. (1989) *J. Magn. Reson. 85*, 608–613.
Morris, G. A., & Freeman, R. (1979) *J. Am. Chem. Soc. 101*, 760–762.
Nirmala, N. R., & Wagner, G. (1988) *J. Am. Chem. Soc. 110*, 7557–7558.
Noggle, J. H., & Schirmer, R. E. (1971) *The Nuclear Overhauser Effect: Chemical Applications*, Academic Press, New York.
Olejniczak, E. T., Dobson, C. M., Karplus, M., & Levy, R. M. (1984) *J. Am. Chem. Soc. 106*, 1923–1930.
Otting, G., Widmer, H., Wagner, G., & Wüthrich, K. (1986) *J. Magn. Reson. 66*, 187–193.
Palmer, A. G., Rance, M., & Wright, P. E. (1991a) *J. Am. Chem. Soc. 113*, 4371–4380.
Palmer, A. G., Cavanagh, J., Wright, P. E., & Rance, M. (1991b) *J. Magn. Reson. 93*, 151–170.
Palmer, A. G., Skelton, N. J., Chazin, W. J., Wright, P. E., & Rance, M. (1992) *Mol. Phys. 75*, 699–711.
Potter, J. D., & Johnson, J. D. (1982) *Calcium and Cell Function* (Cheung, W. Y., Ed.) Vol. II, pp 145–173, Academic Press Inc., New York.
Rigler, R., Roslund, J., & Forsén, S. (1990) *Eur. J. Biochem. 188*, 541–545.
Roder, H., Wagner, G., & Wüthrich, K. (1985) *Biochemistry 24*, 7396–7407.
Seamon, K. B., & Kretsinger, R. H. (1983) *Met. Ions Biol. 6*, 1–52.
Shaka, A. J., Keeler, J., Frenkiel, T., & Freeman, R. (1983) *J. Magn. Reson. 52*, 334–338.
Shaka, A. J., Barker, P. B., & Freeman, R. (1985) *J. Magn. Reson. 64*, 547–552.
Shoji, A., Ozaki, T., Fujito, T., Deguchi, K., Ando, S., & Ando, I. (1989) *Macromolecules 20*, 2860–2863.
Shoji, A., Ozaki, T., Fujito, T., Deguchi, K., Ando, S., & Ando, I. (1990) *J. Am. Chem. Soc. 112*, 4693–4697.
Skelton, N. J., Kördel, J., Forsén, S., & Chazin, W. J. (1990) *J. Mol. Biol. 213*, 593–598.
Skelton, N. J., Akke, M., Kördel, J., Thulin, E., Forsén, S., & Chazin, W. J. (1992a) *FEBS Lett.* (in press).
Skelton, N. J., Kördel, J., Akke, M., & Chazin, W. J. (1992b) *Biochemistry* (submitted for publication).
Smith, G. M., Yu, P. L., & Domingues, D. J. (1987) *Biochemistry 26*, 2202–2207.
States, D. J., Habekorn, R. A., Ruben, D. J. (1982) *J. Magn. Reson. 48*, 286–292.
Stone, M., Fairbrother, W. J., Palmer, A. G., III, & Wright, P. E. (1992) *Biochemistry* (in press).
Svensson, A., Thulin, E., & Forsén, S. (1992) *J. Mol. Biol. 223*, 601–606.
Szebenyi, D. M. E., & Moffat, K. (1986) *J. Biol. Chem. 261*, 8761–8777.
Vogel, H. J., Drakenberg, T., & Forsén, S. (1985) *Biochemistry 24*, 3870–3876.
Vold, R. R., & Vold, R. L. (1976) *J. Chem. Phys. 64*, 320–332.
Vold, R. L., Waugh, J. S., Klein, M. P., & Phelps, D. E. (1968) *J. Chem. Phys. 48*, 3831–3832.
Wagner, G. (1983) *Q. Rev. Biophys. 16*, 1–57.
Willis, B. T. M., & Pryor, A. W. (1975) *Thermal Vibrations in Crystallography*, Cambridge University Press, Cambridge, England.
Zang, L., Laughlin, M. R., Rothman, D. L., & Shulman, R. G. (1990) *Biochemistry 29*, 6815–6820.